

Supporting Information for “Precipitation stable water isotope variability in coastal southwestern Western Australia and its relationship to climate on multiple timescales”

Alan D Griffiths^{1,2}, Pauline C Treble^{1,3}, Pandora Hope⁴, Irina Rudeva^{4,5}

¹ANSTO, Lucas Heights, NSW, Australia

²Centre for Atmospheric Chemistry, University of Wollongong, Wollongong NSW, Australia

³School of Biological, Earth and Environmental Sciences, UNSW, Sydney NSW, Australia

⁴Australian Bureau of Meteorology, Melbourne, Victoria, Australia

⁵P.P. Shirshov Institute of Oceanology, Moscow, Russia

Contents of this file

1. Table S1
2. Figures S1 to S6

References

Dee, D. P., Uppala, S. M., Simmons, A. J., Berrisford, P., Poli, P., Kobayashi, S., ... Vitart, F. (2011). The ERA-Interim reanalysis: Configuration and performance of the data assimilation system. *Q.J.R. Meteorol. Soc.*, 137(656), 553–597. doi:

Corresponding author: A. D. Griffiths, Australian Nuclear Science and Technology Organisation, Lucas Heights, NSW, 2234, Australia. (alan.griffiths@ansto.gov.au)

10.1002/qj.828

Hollins, S. E., Hughes, C. E., Crawford, J., Cendón, D. I., & Meredith, K. T. (2018).

Rainfall isotope variations over the Australian continent – Implications for hydrology and isoscape applications. *Science of The Total Environment*, *645*, 630–645. doi: 10.1016/j.scitotenv.2018.07.082

Hughes, C. E., & Crawford, J. (2012). A new precipitation weighted method for de-

termining the meteoric water line for hydrological applications demonstrated using Australian and global GNIP data. *Journal of Hydrology*, *464–465*, 344–351. doi: 10.1016/j.jhydrol.2012.07.029

Simmonds, I., Keay, K., & Tristram Bye, J. A. (2011). Identification and climatology

of Southern Hemisphere mobile fronts in a modern reanalysis. *J. Climate*, *25*(6), 1945–1962. doi: 10.1175/JCLI-D-11-00100.1

Table S1. Regression between $\delta^2\text{H}$ and $\delta^{18}\text{O}$ in precipitation (local meteoric water line) at Perth and Calgardup Cave. The line of best fit is defined as $y = mx + c$ and both ordinary least-squares (OLS) and precipitation weighted least squares (WLS) are shown; WLS is based on Hughes and Crawford (2012) and Perth data is from Hollins et al. (2018). Daily samples from Calgardup Cave are accumulated to monthly totals before performing the fit, and uncertainties (σ_m, σ_c) are one standard deviation.

	m	σ_m	c	σ_c
<i>2006-2014</i>				
Perth, WLS	7.00	0.34	11.69	1.38
Perth, OLS	6.55	0.30	8.59	1.10
Calgardup Cave, WLS	6.65	0.23	9.21	1.03
Calgardup Cave, OLS	7.40	0.23	11.15	0.96
<i>2006-2018</i>				
Calgardup Cave, WLS	6.92	0.19	10.62	0.87
Calgardup Cave, OLS	7.44	0.18	11.57	0.77

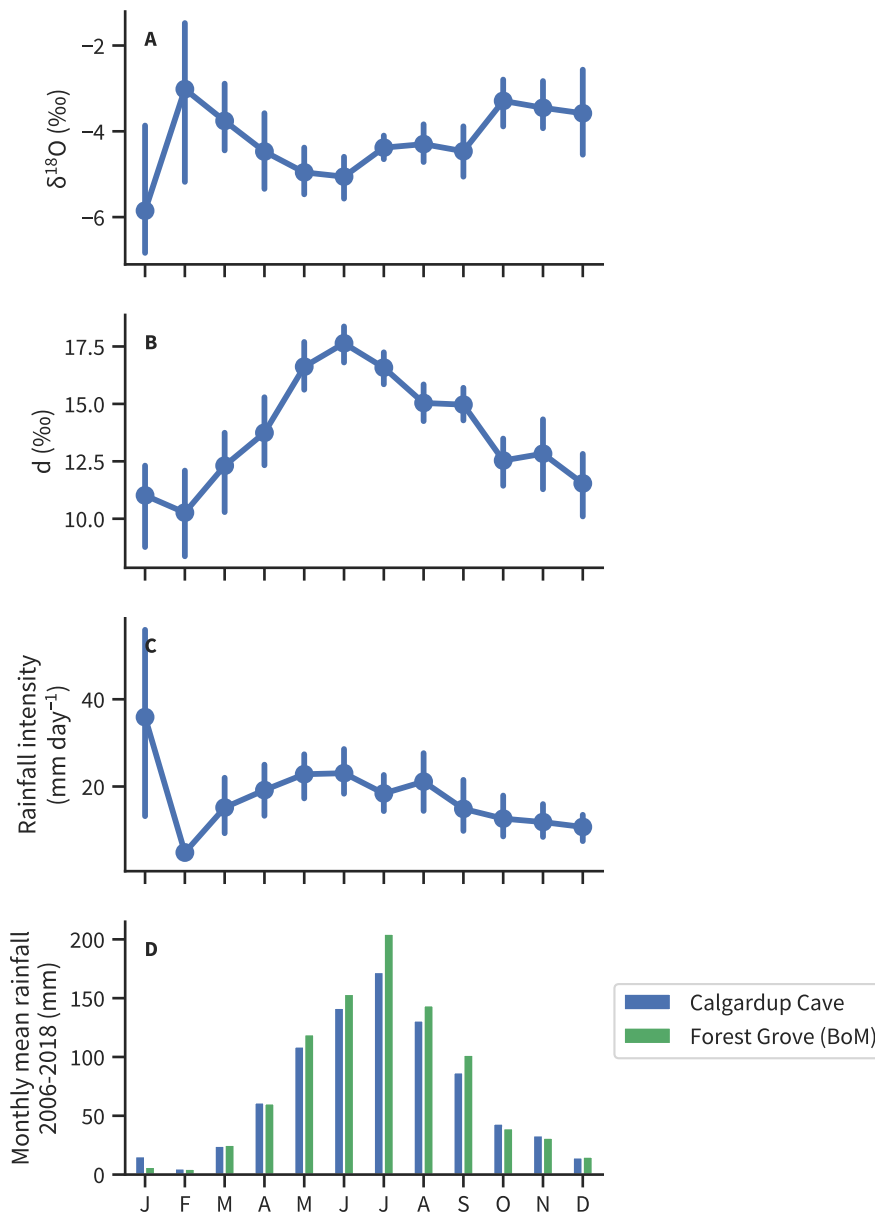


Figure S1. Water isotope and precipitation seasonal cycle from Calgardup Cave, **A** shows $\delta^{18}\text{O}$, **B** shows deuterium excess, d , and **C** shows rainfall intensity per day. In **D**, precipitation measured at Calgardup Cave (excluding events below 2 mm) is compared with the official observations from the nearby Bureau of Meteorology station at Forest Grove. This is computed over the years 2006–18 with year-round data at both sites. Error bars show the 10–90th percentile uncertainty in the mean seasonal cycle, computed by bootstrapping the daily observations and the quantities in panels A–C are amount-weighted.

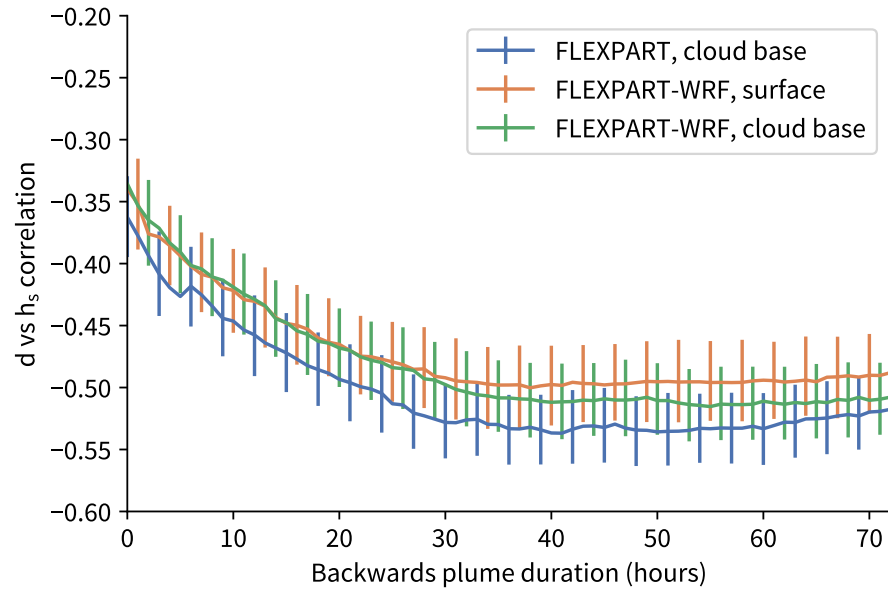


Figure S2. Correlation between deuterium excess in daily precipitation samples and diagnosed h_s as a function of retroplume length for different models (FLEXPART and FLEXPART-WRF). The FLEXPART model is also shown with the receptor at ground level. Error bars show the 10–90th percentile uncertainty, computed by bootstrapping.

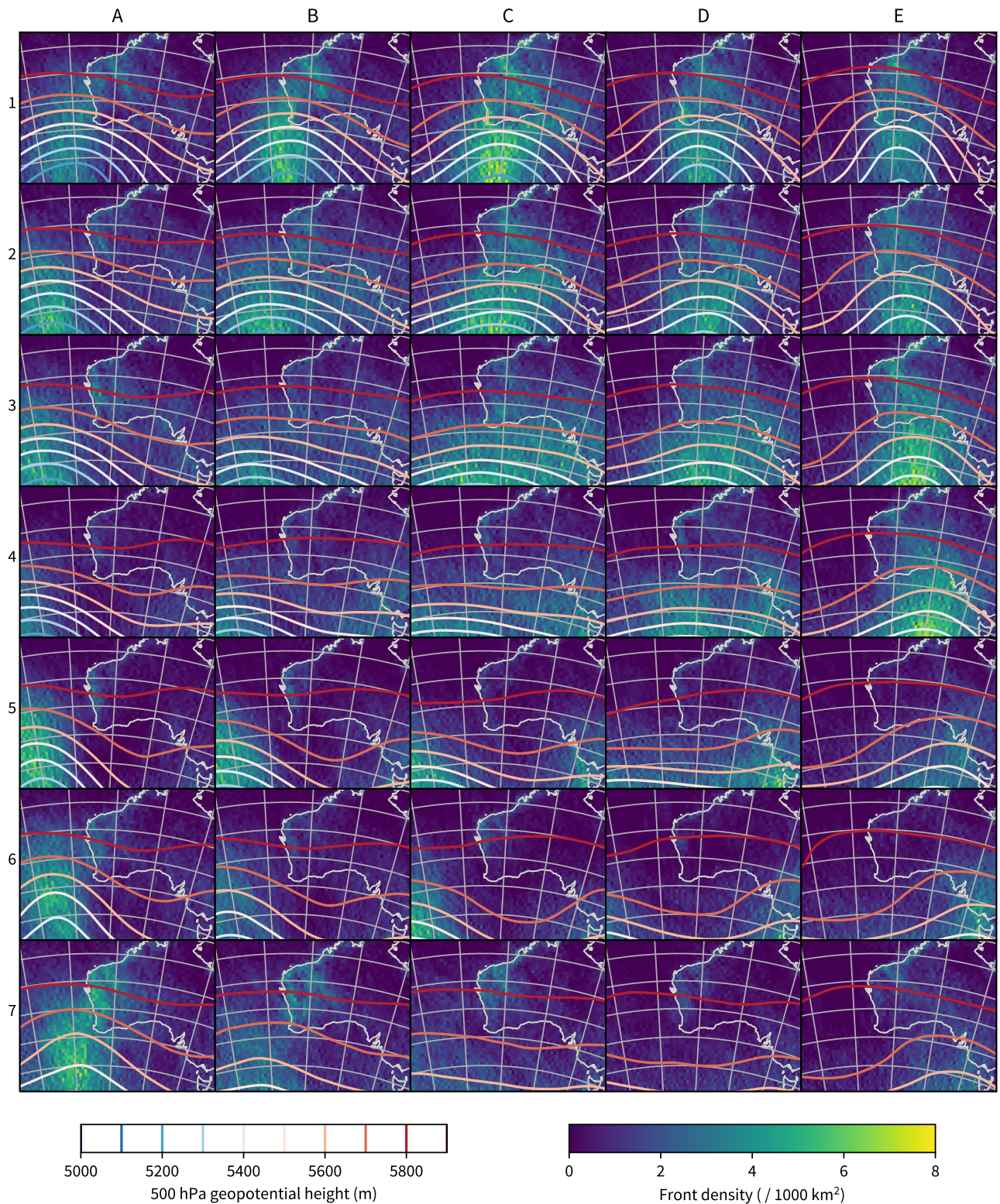


Figure S3. Front density and 500 hPa geopotential height as a function of SOM classification, from ERA-Interim (Dee et al., 2011). Fronts were determined from the surface wind fields using the wind-shift method (Simmonds et al., 2011).

December 3, 2021, 10:43pm

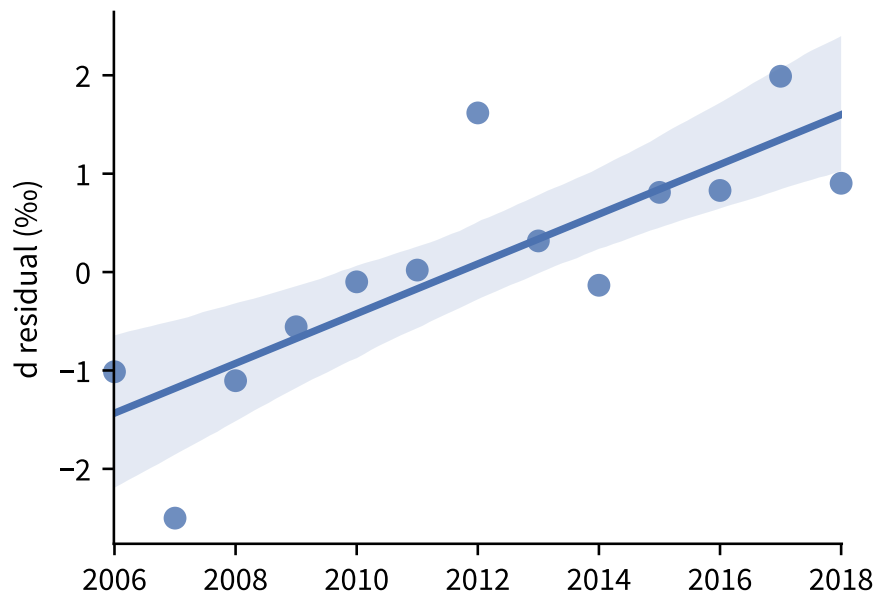


Figure S4. Precipitation weighted Generalized Additive Model (GAM) residuals (observations minus model) for the best-performing d model.

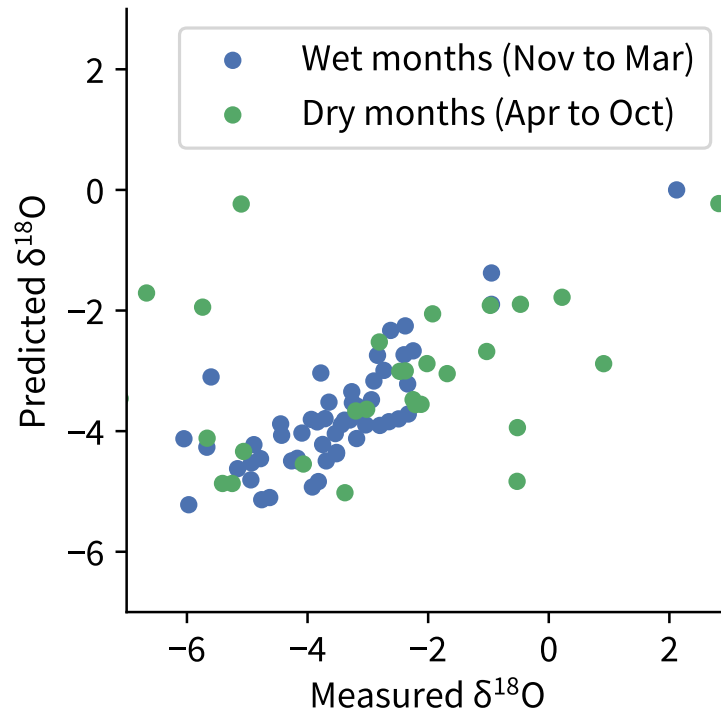


Figure S5. GAM predictions of monthly $\delta^{18}\text{O}$ in rainfall at Perth Airport. The model was trained using daily $\delta^{18}\text{O}$, rainfall, and backwards plumes from Calgardup Cave and then predictions for Perth Airport were generated using the same GAM using the daily rainfall and backwards plumes from Perth Airport before aggregating to monthly precipitation-weighted averages for comparison with observations.

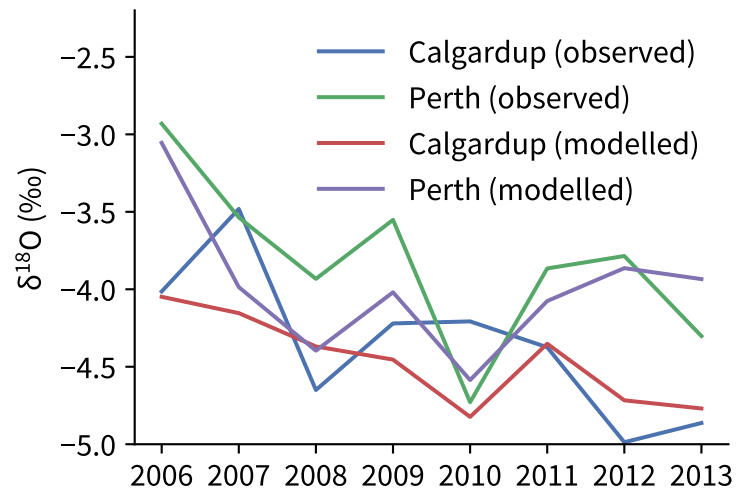


Figure S6. Annual precipitation-weighted $\delta^{18}\text{O}$ from observations and GAM predictions. At Calgardup Cave, daily $\delta^{18}\text{O}$ and rainfall were observed whereas monthly $\delta^{18}\text{O}$ and daily rainfall were observed at Perth Airport.